Optimising P2P Energy Trading using Internet of Things and Agentic AI Cluster Zooming

ANOH, Kelvin, KIPCHUMBA, Benard, VUKOBRATOVIC, Dejan, IKPEHAI, Augustine, OKAFOR, Kennedy Chinedu, MAHARJAN, Sabita and ADEBISI, Bamidele

Optimising P2P Energy Trading Using Internet of Things and Agentic AI Cluster Zooming

Kelvin Anoh, Benard Kipchumba, Dejan Vukobratovic, Augustine Ikpehai, Kennedy Chinedu Okafor, Sabita Maharjan and Bamidele Adebisi

***Abstract*—Artificial intelligence (AI) has become the game changer in smart grids-an enabler of network autonomy, self-healing, and reconfiguration. This study integrates AI and Internet of Things (IoT) to organise peer-to-peer (P2P) energy prosumers into virtual clusters without altering the physical topology of the power network. The aim is to enable an autonomous, scalable and dynamic virtual microgrids (VMG) by leveraging federated learning, agentic AI, AI agents, IoT, and cluster zooming to optimise P2P energy trading costs for prosumers and operational expenditure (OPEX) for network operators, depending on the number of prosumers available. The study employs a central controller AI to coordinate multiple local AI agents. Each AI agent resides in the network server and monitors energy trading traffic for each long-range wide-area network (LoRaWAN) gateway to optimise trading and OPEX costs via cluster zooming achieved by the spreading factor (SF) via adaptive data rate (ADR) mechanism of LoRaWAN. The agentic AI module in the cloud autonomously selects and adapts the network coverage based on SF, via the AI energy trading agent configured in the LoRaWAN access network server, to zoom the clusters (i.e., VMGs) in grid-connected and island modes. The study formulates an energy trading model connecting the physical (*electrical*) and virtual (*telecom*) distances and OPEX in the VMG. With agentic AI-assisted cluster zooming, over 70% of the energy is traded at lower SF. At the same time, the energy costs decrease by 40% in proportion to the network size and the number of prosumers. For the network operator, OPEX reduces by 21% and 38% in base-station power consumption. Ultimately, grid-connected prosumers pay higher charges than their off-grid counterparts. The agentic AI model in this study exemplifies a use case of the 3GPP model of the future 6G network.**

***Index Terms*—Cell zooming, energy trading agent, artificial intelligence, agentic AI, Internet of Things, LoRaWAN, optimisation, peer-to-peer energy trading, virtual microgrids.**

I. Introduction

Artificial intelligence (AI) is a pervasive digital technology that traverses many fields of study, including power networks and smart grids [1], [2]. In most cases, AI complements other digital technologies, such as the Internet of Things (IoT), to enable intelligent solutions [2]. In power distribution networks with embedded generation, AI and peer-to-peer energy trading and sharing (P2P-ETS) are integrated to enhance decentralisation, efficiency, and sustainability in the management of local energy networks [1], [3], [4]. P2P-ETS transforms passive energy consumers into active prosumers [5], [6], provides a platform for selling or sharing excess energy produced or stored by prosumers [3], [7]. When energy prices are high, and the costs of self-consumption from own production and storage are lower, grid power may become less attractive [8], [9]. In that case, energy prosumers with sufficient generation and storage could disconnect from the local energy market (i.e., local power network) turning to self-consumption, leading to voltage instability and high network charges (e.g., Transmission Network Use of System (TNUoS) and Distribution Use of System (DUoS)) for remaining consumers [10]. This grid defection problem is commonly associated with high energy costs and the affordability of energy infrastructure for generation and storage.

In the UK, for example, non-commodity (e.g., distribution, network, government taxes and renewable energy levies) charges constitute about 65% of energy costs and increase every year [11]–[14]. By organising energy prosumers into virtual networks that leverage telecom infrastructure, such problems, including transmission losses and operational costs (OPEX), can be reduced, thereby enhancing energy balance, efficiency, and environmental sustainability [14], [15]. In particular, low-power wide area networks (LP-WANs), such as long-range wide-area networks (LoRaWAN), can be leveraged to enhance network management [7], [15], reduce power losses [16], and lower network fees [14], thereby improving efficiency. By overlaying telecom networks on power networks and enabling data collection, innovative technologies such as AI agents and agentic AI systems [17], [18] based on TinyML [19] can be deployed in smart grids to enhance operational efficiency. Note that AI agents and agentic AI are not synonymous [18]. AI agents perform specific tasks, while agentic AI is an autonomous system that can make decisions and adapt to its environment, often based on inferences from the agents.

LoRaWAN has evolved to become the technology of choice for IoT, 5G, and 6G applications [20]–[22]. While LoRaWAN and LoRa are IoT technologies, the latter allows for point-to-point communication and the former is a networking protocol built on top of LoRa, enabling multiple devices (e.g., prosumers) to connect to a gateway and form a network. Thus, LoRaWAN is more suitable for the present study. It is particularly attractive due to its triple capabilities: low power consumption, low data rates, and wide-area coverage [23]. By leveraging the spreading factor (SF) via its adaptive data rate (ADR) feature, LoRaWAN enables dynamic scaling up or down of the coverage area – a process called *cell zooming* in wireless communication [24]. It was integrated with 6G in the 6G-LoRaGRAN project [25] as a pathway for wide-area coverage enhancement. Cell zooming (e.g., using SF in LoRaWAN) is superior to traditional base transceiver station (BTS) power control due to its simplicity, improved energy efficiency, and ability to respond to fluctuating traffic or resource demands intelligently. In LoRaWAN, the gateway is equivalent to BTS, where SF12 and SF7 offer the longest and shortest ranges, respectively, whereas the reverse holds for data rates. Hence, for a given use case, ADR enables a trade-off among coverage, energy savings and data rate.

However, the SF can be autonomously assigned by the agentic AI (in the cloud) via a local AI energy trading agent (AI-ETA), based on the trading data, similar to using signal quality (e.g.,

K. Anoh, B. Kipchumba and Kennedy Okafor are with the Centre for Future Technologies, University of Chichester, Bognor Regis, PO21 1HR, UK. (Email: {k.anoh,b.kipchumba,kennedy.okafor}@chi.ac.uk).

D. Vukobratovic is with the Faculty of Technical Science, University of Novi Sad, Serbia. (Email: dejanv@uns.ac.rs).

A. Ikpehai is with the School of Engineering & Built Environment, Sheffield Hallam University, Sheffield, United Kingdom. (Email: a.ikpehai@shu.ac.uk).

S. Maharjan is with the Department of Informatics, University of Oslo, Norway. (Email: sabita@ifi.uio.no)

B. Adebisi is with the School of Engineering, Manchester Metropolitan University, Manchester, M1 5GD, UK. (Email: b.adebisi@mmu.ac.uk).

received signal strength indicator (RSSI), signal-to-noise ratio (SNR) and data rate) [26]. Switching SF using AI reduces packet loss and improves energy efficiency in LoRaWAN by at least 30% in static and dynamic modes compared to using ADR [27], [28]. Employing agentic AI, AI-ETA, AI-ADR and IoT in cell zooming is, therefore, a powerful and cost-effective way to dynamically adjust communication network coverage in real-time based on the number of active prosumers. It mitigates over-provisioning of network resources and unnecessary costs. In community energy networks, cluster zooming with IoT is a promising technique for optimising operating costs, energy costs, power losses, and the carbon footprint. It has been previously shown that employing ICT to organise energy prosumers into virtual microgrids (VMG), reduces energy trading cost [7], [15], [23], [29]. This study proposes AI-based SF switching in LoRaWAN to manage cluster zooming in the transactive energy system formed by VMGs, without altering the physical architecture of the power network. Unlike [30] seeking seller profits, SF-enabled cluster zooming, via agentic AI and AI-ETA, optimises the number and distance of prosumers at each trading session, reducing trading costs and motivating passive energy consumers to become active prosumers. The scheme is also useful for grid resilience as it enables rapid recovery from network failures or over-subscription of telecom network capacity. Our main contributions in this study are

- modelling, design and implementation of agentic AI and AI-ETA to control VMGs based on energy trading data. IoT, AI agents and agentic AI are proposed to predict VMG (or coverage) size, based on energy trading data that are integrable in the present 5G and beyond;
- elastic trading networks in which energy prosumers are logically grouped into virtual networks and can self-adjust to improve operational efficiency. We evaluate operational cost performances for the energy trading models, including the network charges;
- dynamic availability and coverage of overlaying IoT networks in P2P trading system. The hybrid model combines a Poisson-point process with the flexibility of SF controlled by agentic AI and AI agents in LoRaWAN;
- dynamic discovery of active prosumers based on the traffic density at the LoRaWAN station in each trading session to minimise non-commodity costs;
- trading cost model that incorporates the distance of a seller from a buyer in the network fees. The cost model provides an analytical relationship connecting the physical (*electrical*) and logical (*communication*) distances. When energy prosumers are reasonably separated, the energy trading cost is higher, thus encouraging local energy trading, which reduces emissions and power losses.

The unique feature of SF in LoRaWAN is the motivation to investigate a new model of energy trading among prosumers. However, unlike existing related works that explore opportunities for trading cost optimisation [7], [31], our model follows a nonlinear energy trading cost function that is strictly convex in nature. The rationale is that nonlinear energy trading models are widely used in practical systems [32]. To reduce the energy trading cost for consumers, we then formulate and solve the optimisation problem of the energy cost model in a distributed fashion, as the energy demands of consumers are independent.

The system model is presented in Section II and the proposed cost model in Section III. The simulation results are discussed in Section IV with the conclusion following.

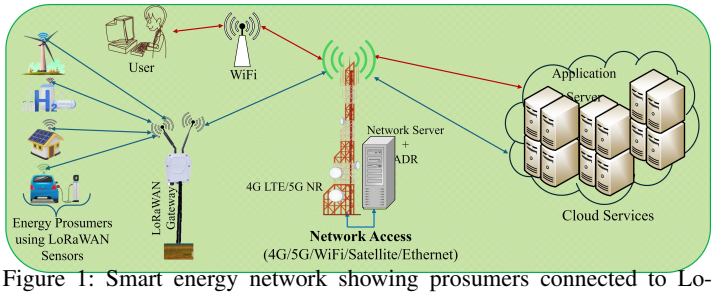

Figure 1: Smart energy network showing prosumers connected to LoRaWAN gateway using LoRaWAN sensors [26].

II. System Model

The IoT networks enable prosumers to exchange real-time data—the basis for metering, P2P trading and transaction settlement. With current IoT and cellular (4G/5G) networks, energy prosumers' facilities equipped with LoRaWAN sensors can be remotely monitored by an energy trading network manager (user) as shown in Figure 1. Each 4G/5G BTS may connect k LoRaWAN gateways, while a large trading area might encompass n cellular BTSs. Consider a large P2P energy trading area with prosumers randomly distributed therein. In P2P-ETS, prosumers remain physically organised (connected to LV distribution network) and can can be logically grouped into virtual clusters via IoT devices such as LoRaWAN, as shown in Figure 2 (Plane 1), that are connected to a wide area network (WAN) such as cellular network (4G/5G/6G) or satellites (Plane 2) [14]. Logical grouping refers to organising prosumers into clusters based on overlaying communication network and data exchanged rather than hard physical boundaries or location on the power grid alone. The WAN BTSs connect to the cloud (Plane 3). Practically, LoRaWAN covers a distance up to 5 km in non-line of sight (NLOS) and 30 km in LOS [33]. It can increase or reduce the P2P cluster size depending on traffic density by adjusting its physical attribute, SF (Plane 4). In this study, we envision an SF controlled by an AI-ETA on the network server, which depends on the number of prosumers and other energy trading data in a VMG. We assume that the clusters (or VMGs) formed by using the AI-ETA experience tolerable interference at the edges of the VMG networks. The AI-ETA enables neighbouring peers to discover each other and trade energy through a power distribution network. All prosumers within the service area of an AI-ETA have the capability to both produce and consume energy. In this study, the AI-ETA is enabled by LoRaWAN due to its scalability, energy consumption, dynamic coverage and packet loss merits over other LP-WANs [20], [34]. Energy prosumers can use their energy trading client (ETC) as a local gateway (e.g., LoRaWAN sensors or other sensors with Wi-Fi, BLE, or ZigBee via a multi-protocol gateway) to connect wirelessly to LoRaWAN. We consider packet loss because it increases uncertainty, reduces the amount of energy sold, and increases total energy cost [34]. Additionally, all prosumers are assumed to be physically connected to an energy distribution network and are therefore permitted to trade energy among themselves.

We represent the physical connectivity among the prosumers using an energy trading graph $G = (P, \mathcal{E})$, where $P = \{\mathcal{P}_1, \cdots, \mathcal{P}_N\}$ is the set of prosumers, N is the total number of prosumers in the VMG network and $\mathcal{E} \subseteq P \times P$ is the set of edges. Let all prosumers that sell energy in a given trading interval, t, be denoted by $\mathcal{S}_i(t) \in P, i \in \mathcal{N}$, where $\mathcal{N} = \{1, \cdots, N\}$ is

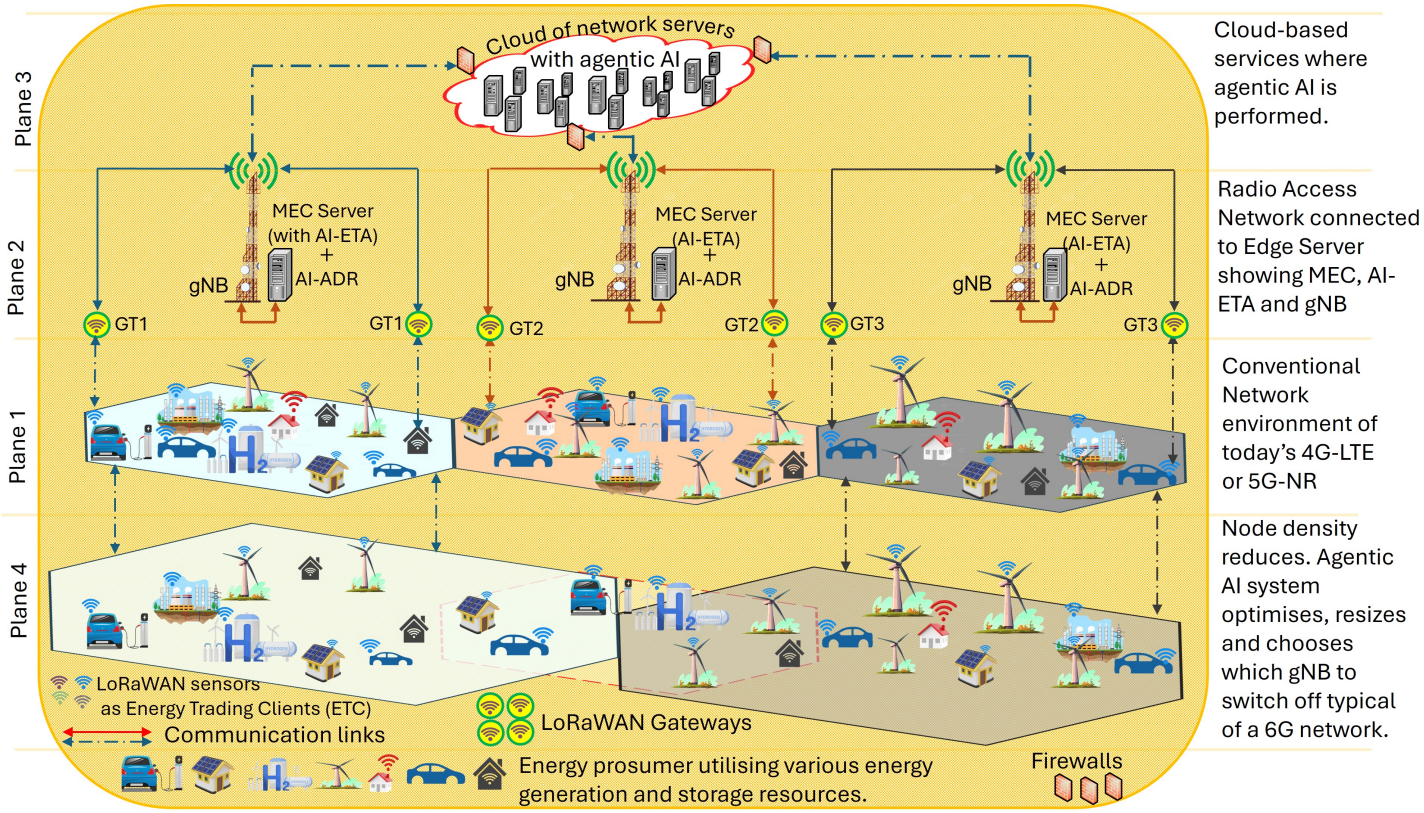

Figure 2: Proposed future 6G-enabled P2P energy trading network, with energy trading AI agents and agentic AI orchestration of IoT (e.g., LoRAWAN) network resources and adaptive coverage management [26].

the set of indices. We further denote $\mathcal{B}_j(t) \in P, j \in \mathcal{N}_i$ where $\mathcal{N}_i \in \mathcal{N}$ is the set of indices of energy consumers that are buying energy from seller i. Both $\mathcal{S}_i(t)$ and $\mathcal{B}_j(t)$ are subsets of all prosumers in one VMG, and thus constitute all the P prosumers and $\mathcal{S}_i(t) \cap \mathcal{B}_j(t) = \varnothing$ [29].

Prosumers can generate energy from various resources and engage in P2P trading. This makes it crucial to consider a holistic trading model that incorporates both renewable and non-renewable energy resources. In general, each producer generates a total of $E_i^{(g)}(t)$ amounts of energy and consumes $E_i^{\min}(t) \leq e_{ii}(t) \leq E_i^{\max}(t)$ amount of energy, where $E_i^{\min}(t)$ and $E_i^{\max}(t)$ are the minimum and maximum energy required by prosumer $\mathcal{S}_i(t)$, respectively. That is, the seller consumes $e_{ii}(t) \in E_i^{(g)}(t)$ and sells the remaining $x_{ij}(t)$ to its $\mathcal{B}_j(t)$ neighbours. Note that the total energy sold by a prosumer is derived from the excess amount of energy generated or stored. In other words, the total excess energy declared by prosumer i at trading period t is

$$y_i(t) = E_i^{(g)}(t) - e_{ii}(t) \;\; \forall i \in \mathcal{N}, \; t = 1, \cdots, T. \tag{1}$$

For energy prosumers, i, without energy storage capability, they must sell all $y_i(t)$, although power losses reduce the actual amount delivered. Following [16], the power delivered to prosumer j by prosumer i will be less of the power losses, $\phi_{ij}(x_{ij}) = \sum_j \gamma_i x_{ij}^2$ so that, (1) can be rewritten as

$$\sum_{j \in \mathcal{N}_i} x_{ij}(t) = y_i(t) - \sum_{j \in \mathcal{N}_i} \gamma_i x_{ij}^2(t), \; \forall i \in \mathcal{N} \tag{2}$$

where γ_i are the loss-coefficients. If $X_j = [x_1, x_2, \cdots, x_{\mathcal{N}}]$ is the energy sold to j-th prosumer in one VMG, then

$$\mathbf{X} = [X_1, X_2, \cdots, X_{\mathcal{N}_i}]^T \tag{3}$$

represents the total energy traded within one VMG at time t, and $[\cdot]^T$ denotes the transpose of $[\cdot]$. The payoff received by i from j due to the $x_{ij}(t)$ amount of energy sold is denoted as $p_{ji}\left(x_{ij}(t)\right)$. Note that, as energy flows from $\mathcal{S}_i(t)$ to $\mathcal{B}_j(t)$ i.e. $(i \rightarrow j)$, then money is paid by buyer $\mathcal{B}_j(t)$ to seller $\mathcal{S}_i(t)$ i.e. $(j \rightarrow i)$, hence the ordering of indices is x_{ij} and p_{ji}, respectively. We assume that the number of prosumers is constant at each trading period; this assumption enables effective modelling of the scheme to cover electric vehicles (EVs) that may change locations. With a VMG, a common energy price can be assigned per kWh traded.

A. Energy Trading Cost Model

In [7], [23], it was shown that the total energy trading cost includes generation, distribution and emission costs. The total payout to seller i from j^{th} buyer is

$$\mathcal{T}_j\left(\{x_{ij}\}_{i \in \mathcal{N}}\right) = \mathcal{C}_{ji}(x_{ij}(t)) + I_{ji}(x_{ij}(t)) + \tau_{ji}(x_{ij}(t)) \tag{4}$$

where $\mathcal{C}_{ji}(x_{ij}(t)) = \sum_{i \in \mathcal{N}} a_{ji} x_{ij}^2 + \sum_{i \in \mathcal{N}} b_{ji} x_{ij}$ is the total generation cost, $I_{ji}(x_{ij}(t)) = \sum_{i \in \mathcal{N}} \alpha_{ji} x_{ij}^2 + \sum_{i \in \mathcal{N}} \beta_{ji} x_{ij}$ is the nonlinear emission cost and $\tau_{ji}(x_{ij}(t)) = \sum_{i \in \mathcal{N}} \tau_{ji} x_{ij}$ is the distribution charges. Practical energy cost models are nonlinear (e.g. quadratic as in [32]), unlike the linear model described in [7]. When prosumers trade renewable energy resources, we assume that there are no greenhouse emissions; i.e., we set $I_{ji}(x_{ij}(t)) = 0$ in (4), otherwise $I_{ji}(x_{ij}(t)) \neq 0$.

If the energy cost of operating the base station (LoRaWAN gateway) is considered, then (4) will be rewritten as:

$$\begin{aligned}\mathcal{T}_j\left(\{x_{ij}\}_{i \in \mathcal{N}}\right) =& \mathcal{C}_{ji}(x_{ij}(t)) + I_{ji}(x_{ij}(t)) + \tau_{ji}(x_{ij}(t)) \\ &+ \sum_{i \in \mathcal{N}} C_{ji}(x_{ij}(t))\end{aligned} \tag{5}$$

where $C_{ji}(x_{ij}(t))$ is the communication cost (i.e., cost required to operate the base station). Based on the proportion of time, Δt,

that each of the k LoRaWANs was used to transmit the P2P-ETS data d_{ij}^k required to process trading information about $x_{ij}(t)$, then the energy required by the LoRaWAN can be represented as:

$$\mathrm{E}_k = P_{t,k}(x_{ij}) \cdot \Delta t_k, \qquad k = 1, 2, \cdots, \mathcal{M} \tag{6}$$

where $P_{t,k}(\cdot)$ is the transmit power (W) required to transceive d_{ij}^k while selling x_{ij} and $\mathcal{M}$ is the number of VMGs. The energy drawn from each LoRaWAN gateway depends on the node density at each VMG within a given trading period, t. If the data rate $R = d_{ij}^k/\Delta t_k$, then

$$\mathrm{E}_k = P_{t,k}(x_{ij}) \cdot \frac{d_{ij}^k}{R}, \qquad k = 1, 2, \cdots, \mathcal{M}. \tag{7}$$

If d_{ij}^k is charged at π_e, then the cost of data transmitting (Communication Network Use of System (CNUoS)) d_{ij}^k to sell $x_{ij}(t)$ units of energy becomes:

$$\begin{aligned} C_{ji}^k(x_{ij}) &= M_0^k + \pi_e \mathrm{E}_k \\ &= M_0^k + \pi_e \cdot P_{t,k}(x_{ij}) \cdot \frac{d_{ij}^k}{R}, k = 1, 2, \cdots, \mathcal{M} \end{aligned} \tag{8}$$

where M_0^k is the maintenance cost. If $N = \mathcal{N}_i + \mathcal{N}$ prosumers share the LoRaWAN station at Δt period, then per user cost

$$C_{ji}^k(x_{ij}) = \frac{1}{N}\left(M_0^k + \pi_e \cdot P_{t,k}(x_{ij}) \cdot \frac{d_{ij}^k}{R}\right). \tag{9}$$

With the agentic AI and cluster zooming paradigm, the LoRaWAN will dynamically turn ON or OFF, thus $P_{t,k}(\cdot)$ includes idle and active power consumption for the LoRaWAN station as

$$P_{t,k}(x_{ij}) = z_k \cdot P_{idle}(x_{ij}) + \xi_k \cdot P_{active}(x_{ij}) \tag{10}$$

where $P_{idle}(\cdot)$ is the static power used by the base station (LoRaWAN gateway) for baseband processing or cooling, $P_{active}(\cdot)$ is the dynamic power consumed when in an active state, which varies depending on the SF used such as SF7, SF8, etc. We introduced the binary values $z_k \in [0, 1]$, $\xi_k \in [0, 1]$ and $z_k \neq \xi_k$ to indicate ON or OFF states. Consequently, the OPEX can be determined as

$$\mathrm{OPEX} = \sum_{k \in \mathcal{M}} C_{ji}^k(x_{ij}). \tag{11}$$

While the OPEX can be evaluated via $C_{ji}^k(\cdot)$ in LoRaWAN or other communication networks, the impact of the ADR and SF mechanism (i.e., cluster zooming, node density and coverage) can be explored through $\tau_{ji}(\cdot)$.

B. Agentic AI As an Autonomous System

We propose a controller-agent model of an agentic AI system with a central controller and multiple AI agents, as shown in Figure 3. While multi-agent agentic AI systems involve multiple agents operating on a single environment, this study instead presents a central controller (in the cloud) and a single agent per LoRaWAN (at the edge). Consequently, our model is not prone to anti-competition behaviour (e.g., agent collusion) problem inherent in multi-agent agentic AI systems [35] which could be mitigated with blockchain in P2P-ETS [4], [36]. Traditional AI models are trained using data (online or offline) to perform specific tasks when given specific instructions [18]. In this study, the AI-ETA uses reinforcement learning based on the Q-learning model to learn node-density based on traffic and sends its inference to the agentic AI system in the cloud, as shown in Figures 2 and 3. Since an agentic AI module, such as software (e.g., APIs) or hardware (e.g., robots, drones), can autonomously make decisions and adapt to environmental changes to achieve specific goals [17], herein, the agentic AI system is a software-defined in the cloud.

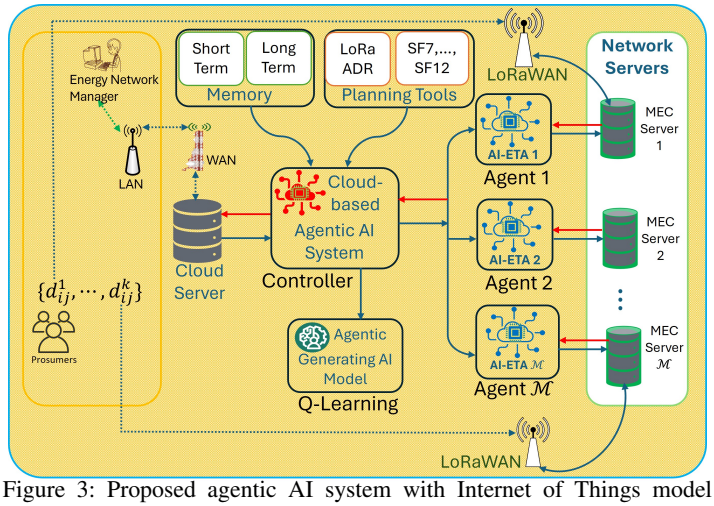

Figure 3: Proposed agentic AI system with Internet of Things model including multiple local energy trading AI agents.

As shown in Figure 3, the agentic AI framework is modelled as a multi-agent system in which the edge AI-ETA learns and reports the node density based on the traffic status of each LoRaWAN gateway to the central controller. In the implementation, we created a Q-learning instance and applied it to each AI-ETA and the core networks, thereby making the proposed agentic AI system lightweight and reducing costs. Using the reasoning engine, the agentic AI processes, decides, and plans its actions to increase, retain, or reduce coverage based on the node-density status received from the trading area. As an autonomous system, the AI-ETA fetches energy trading data from the packets arriving in the mobile edge computing (MEC) server shown in Figures 2 and 3 and feeds the results to an agentic AI system in the cloud [37]. Since energy trading prices are private [38], an AI-ETA cannot use energy prices in the SF configuration. With a global knowledge of the trading area, the agentic AI (in the cloud) determines whether the coverage should be changed and then issues instructions to change the SF to local AI agents (i.e., AI-ETA) in the MEC server of individual LoRaWAN stations. Based on the results, AI-ETA switches the SF to minimise energy network charges and redundant LoRaWAN gateways turned OFF, saving OPEX. As WAN gateways are decentralised and so are the network (MEC) servers, blockchain can be used to authenticate prosumers and AI-ETA, thus enhancing trust and security in the network [4], [36].

6G will be user-oriented (unlike the service-oriented 5G network) and retain the next-generation Node-B (gNB) of the 5G network, albeit with added functionalities. The radio access network (RAN) and core networks will be more complex, self-organising, intelligent and cost-effective than the 5G networks [39], [40]. In Rel-18, 3GPP introduced AI/ML in the RAN of 5G network, with the RAN3 working group working to include AI4Net and Net4AI in Rel-19 [41]. While agentic AI will be included in the network server (i.e., RAN) according to 3GPP in 6G [41], the 5G/6G network server does not bear the global knowledge of the P2P trading area, thus the agentic AI is included in the cloud in this study. Thus, integrating agentic AI in the core network (e.g., cloud) and AI agents in the RAN (e.g., gNB) to support P2P energy trading, as shown in Figures 2 and 3 represents the next wave of cutting-edge capabilities in smart energy systems. This distributed technique can be deployed with an evolved Node-B (eNB) of a 4G network, a next-generation eNB (ng-eNB) of a non-standalone 5G network, and a gNB of

a standalone 5G network, leveraging the upgrade path between different generations of cellular technologies.

C. Agentic AI-Assisted Cell Zooming For P2P Energy Trading

High energy prices, combined with low production and storage costs, can make grid power optional for some prosumers and lead to grid defection. For example, some energy prosumers with onsite generation (e.g., solar panels, wind, biomass, etc.) and storage (e.g., battery, EV or flywheel) facilities disconnect from the grid and switch to self-consumption of their own energy, thus increasing the non-commodity charges for remaining prosumers and causing grid instability [8]–[10]. Regarding high energy prices, the primary driver is network charges [10]. Given the prosumer churn problem, LoRaWAN AI-assisted cell zooming can be used to discover and increase the number of energy prosumers within a coverage area, thereby reducing high energy costs.

Unlike other technologies, LoRaWAN achieves cell zooming using its SF via ADR. For a given SF, let $\{r_k : k \in \mathcal{M}\}$, where $\mathcal{M} = 1, 2, \cdots, M$ number of VMGs, be the LoRaWAN coverage [42], [43], then

$$r_k = \left(\frac{c}{4\pi f}\right)^{2/\mu} \cdot \sqrt[\mu]{\frac{2^{\text{SF}}\mathcal{P}_t}{\gamma_0 \xi k_B \mathbb{T} W}} \qquad \forall k \in \mathcal{M} \tag{12}$$

where $f = 868$ MHz is the frequeny, $\mathcal{P}_t = 14$dB (decreasing by 2dB per SF) is the maximum transmit power in Europe [44, p. 33], μ is the path-loss exponent (2 for free space, 3 for urban centres and 6 for high rising shadowing), γ_0 is the desired SNR, c is the speed of light in a vacuum, $\xi = 6$dB is the noise figure, k_B is the Boltzmann constant, $\mathbb{T}$ is the temperature of the environment and W is the bandwidth. The cost model in (4) accounts for the pay-off received by prosumer i from $\{j \in \mathcal{N}_i\}$ within r_k. Interested readers are referred to our previous work [20] for a comprehensive analysis of LoRaWAN performance based on actual OEM datasheets.

Figure 2 illustrates an energy trading area overlaid with IoT networks (e.g., LoRaWAN) that communicate with prosumers and the cloud. In the design, the communication network is assumed to be secure for agents to trade freely leveraging the 128-bit Advanced Encryption Standard of LoRaWAN IoT, firewalls and blockchain integration for prosumer and agent authentication. Under favourable energy prices, each LoRaWAN IoT forms a VMG with a low SF (e.g., SF7), thereby reducing network charges and OPEX (Figure 2 Plane 4). As the market becomes unbearable or EVs move away (Figure 2 Plane 4), network charges increase for the remaining prosumers. LoRAWAN devices zoom their cluster sizes (by switching from SF7 to a higher SF, e.g., SF10) to discover more prosumers, thus reducing charges while redundant LoRAWAN nodes enter sleep mode or switch off (Figure 2 Plane 4). Unlike mobile cellular networks [24], where users' positions fluctuate in space and time, energy prosumers are treated as static nodes, except for EVs, which can join or leave the network, depending on the perceived benefits. Notably, as the number of prosumers increases, the network charges decrease due to the cell zooming phenomenon [8]–[10], [24]. The redundant LoRaWAN nodes (and the AI-ETA) can be switched off or placed in sleep mode by the agentic AI, thereby reducing OPEX and energy consumption. To minimise the impact of adjacent cell interference, other VMGs can also switch to a lower SF (e.g., Figure 2 Plane 1). To minimise instability, ideal power networks should have a low prosumer defection rate. Thus, the AI agent can be trained to follow realistic energy market demands, and IoT devices will send limited packets (e.g., 50 packets/day [34]).

In the proposed model, each prosumer will be charged based on the *electrical distance* ℓ_{ij} separating $\mathcal{S}_i(t)$ and $\mathcal{B}_j(t)$ inside k-th VMG. In power networks, ℓ_{ij} can be evaluated under impedance $Z_{\ell_{ij}} = R + jX_L$, where $R = \rho_R(\ell_{ij}/A_{\ell_{ij}})$ with $\rho_R =$ resistivity, $A_{\ell_{ij}} =$ cross-sectional area of the wire delivering the power, and $X_L = 2\pi f L$ is the inductive reactance per unit length (e.g., Ω/km or Ω/mile) with $L = \kappa\ell_{ij}$ is the inductance of the wire and κ is a constant [45], [46]. So, $Z_{\ell_{ij}}$ increases with ℓ_{ij}. It follows that ℓ_{ij} depends on the size of the VMG, r_k (*or the communication distance*), which we will assume to be the diameter of k-th VMG throughout this paper [26]. In that case, the transmission cost part of (4) becomes

$$\tau_{ji}x_{ij}(t) = \theta_{ji}\ell_{ij}x_{ij}(t)\ \forall i \in \mathcal{N}, j \in \mathcal{N}_i,\ t = 1, \cdots, T, \tag{13}$$

where θ_{ji} is the transmission price of x_{ij} per unit distance. From (4), if $\hat{a}_{ji} = a_{ji} + \alpha_{ji}$, $\hat{b}_{ji} = b_{ji} + \beta_{ji} + \theta_{ji}\ell_{ij}$ and $f_{ij}(x_{ij}) = \hat{a}_{ji}x_{ij}^2 + \hat{b}_{ji}x_{ij}$, then (4) becomes

$$\mathcal{T}_j(\{x_{ij}\}_{i\in\mathcal{N}}) = \sum_{i\in\mathcal{N}} f_{ij}(x_{ij}), \quad j \in \mathcal{N}_i. \tag{14}$$

From (14), it is easy to envisage the *selfish* goals of each prosumer, namely, the consumer would like to minimise the cost it pays by minimising (14) while the producer maximises the pay-off it receives by maximising (14). Such a problem can be treated using Game Theory [14].

D. Cell Zooming, Traffic Intensity and Node Density

Based on SF, LoRaWAN covers a distance r_m and thus the respective distance of the $\mathcal{S}_i(t)$ from $\mathcal{B}_j(t)$ depends on $r_m, m \in \mathcal{M}$. In the literature, several methods exist for determining ℓ_{ij} based on r_m for uniformly distributed random nodes confined to a geometric shape, as seen in [47], [48]. In this study, we consider the case of prosumers randomly distributed in the VMG to estimate ℓ_{ij}. Conventional cellular networks are usually modelled using regular hexagons as shown in Figure 2 or as concentric circles. For simplicity, we assume that each cell formed by SF is a hexagon. Let $r_i, i \in \mathcal{N}$ be the reference distance of node i from the centre of the cell formed by LoRaWAN, given SF, and $\mathcal{F}(r_i) = 6r_i$ (or $2\pi r_i$ for circles) is the probability density function (PDF) of the nodes uniformly distributed in the cell. The average distance between $\mathcal{S}_i(t)$ and $\mathcal{B}_j(t)$ can be expressed as $(\forall i, j \in \mathcal{N})$

$$\ell_{ij}^{\hexagon} = \frac{\int_{r_i=0}^{r_i=r_m} r_i\mathcal{F}(r_i)dr_i}{\int_{r_i=0}^{r_i=r_m} \mathcal{F}(r_i)dr_i} = \frac{6\int_{r_i=0}^{r_i=r_m} r_i^2 dr_i}{6\int_{r_i=0}^{r_i=r_m} r_i dr_i} = \frac{2r_m}{3} \tag{15}$$

where $\hexagon$ denotes hexagon and $m \in \mathcal{M}$. From [26], the maximum separation between $\mathcal{S}_i(t)$ from $\mathcal{B}_j(t)$ is $2r_m$, thus

$$\ell_{ij} = 2 \times \frac{2r_m}{3} = \frac{4r_m}{3}. \tag{16}$$

Henceforth, we will use (16) to represent the average distance separating $\mathcal{S}_i(t)$ from $\mathcal{B}_j(t)$ within a VMG.

Let the traffic density received at the AI-ETA be proportional to the number of prosumers in the network. We can model the node density in a VMG for cell zooming based on the traffic density received at each LoRaWAN at a given trading period. To do this, let the active node distribution follow a Poisson distribution model [49], for example, the Poisson-point process (PPP), which can be expressed as

$$P_{\text{SF}}\{|\mathcal{N}| = n_t\} = \frac{\Lambda_{\text{SF}}^{n_t}}{n_t!} e^{-\Lambda_{\text{SF}}}, n_t = 0, 1, 2, \cdots \tag{17}$$

where n_t is the number of times messages arrive at the ETA per trading interval and Λ_{SF} is the expected number of prosumers. As Λ_{SF} varies in the P2P energy market, the scheme enables dynamic node-density coverage via SF over a given trading period. The expected number of prosumers per VMG $\mathbb{E}[\mathcal{N}] = \Lambda_{\text{SF}} = \lambda A_{\text{SF}}$, where $A_{\text{SF}} = 3\sqrt{3}{\ell_{ij}}^2/4$ is the area of a regular hexagonal VMG.

III. Energy Cost Optimisation With AI-Assisted LoRaWAN Cell-Zooming

Usually, when prosumers derive no benefits from the grid, those with sufficient generation and storage capacity are motivated to disconnect from the grid [8]–[10]. This grid defection problem increases network costs for consumers remaining in the network [10]. Prosumers with limited storage will sell all their excess energy.

A. Prosumers with Limited Demand Capacity

Let $\sum_i x_{ij} \geq \mathbb{C}_j$, with $\mathbb{C}_j$ as demand cap of j. Typically, (4) can be formed into a convex optimisation problem that can be solved centrally (e.g., by the AI-ETA) per VMG. Let the optimisation problem **P1** be of the form

$$\textbf{P1:} \quad \min_{\{x_{ij}\}_{i,j\in\mathcal{N}}} \sum_{j\in\mathcal{N}_i} \mathcal{T}_j\left(\{x_{ij}\}_{i\in\mathcal{N}}\right)$$

$$\text{subject to: (2)} \tag{18a}$$

$$\sum_{i\in\mathcal{N}} x_{ij} \geq \mathbb{C}_j, \ \forall j \tag{18b}$$

$$x_{ij} \geq 0, \ \forall i \in \mathcal{N}, \ \forall j \in \mathcal{N}_i. \tag{18c}$$

In **P1**, constraint (18a) is used by the AI-ETA as a decision criterion to eliminate or permit a prosumer to join in the trade. One way to reduce energy costs is to minimise consumption. For example, demand response campaigns can help minimise energy consumption by shifting flexible loads to off-peak periods, thereby avoiding excessive charges. We can find the optimal cost by first expressing the Lagrangian of **P1** as

$$\begin{aligned}\mathcal{L}(x,\lambda,\eta) = &\sum_{i\in\mathcal{N}}\sum_{j\in\mathcal{N}_i} f_{ij}(x_{ij}) - \sum_{j\in\mathcal{N}} \eta_j\Big(\sum_{i\in\mathcal{N}_i} x_{ij} - \mathbb{C}_j\Big) \\ &+ \sum_{i\in\mathcal{N}} \lambda_i\Big(y_i - \sum_{j\in\mathcal{N}_i} x_{ij} - \sum_{j\in\mathcal{N}_i} \gamma_i x_{ij}^2\Big)\end{aligned} \tag{19}$$

where $\boldsymbol{\lambda} \in \mathbf{R}_+^{|\mathcal{N}|}$ and $\boldsymbol{\eta} \in \mathbf{R}_+^{|\mathcal{N}_i|}$ are the Lagrangian multipliers (or price variables) associated with the excess energy capacity constraint (i.e. (18a)) and the availability constraint (i.e. (18b)), respectively. Clearly, we can observe that (19) is convex and the model can be solved centrally by the AI-ETA. Among the methods of solving (19) are the interior-point methods (e.g. [50]), and they are all centralised algorithms.

However, each prosumer's energy information is private. The AI-ETA can not solve the optimisation problem (19) without this information [4], [6], [38]. In addition, this approach could make the energy pricing information stale, thus causing prosumers to lose offers. Since the P2P prosumers are distributed, they can solve this problem in a distributed fashion of the form

$$\textbf{D1:} \quad \mathcal{D}(\lambda,\eta) = \inf_{\{x_{ij}\}_{i,j\in\mathcal{N}}} \mathcal{L}(x,\lambda,\eta) \tag{20a}$$

$$= \Psi(x_{ij}) + \Phi(x_{ij}) \tag{20b}$$

where $\Psi(x_{ij}) = \sum_{i\in\mathcal{N}}\sum_{j\in\mathcal{N}_i} \psi_{ij}(\lambda_i,\eta_j)$, $h(x) = (-\lambda_i - \eta_j)x_{ij} - \lambda_i\gamma_i x_{ij}^2$, $\Phi(x_{ij}) = \sum_{i\in\mathcal{N}} \lambda_i y_i + \sum_{j\in\mathcal{N}_i} \eta_j \mathbb{C}_j$ and

$$\psi_{ij}(\lambda_i,\eta_j) = \textbf{arg min}_{x_{ij}\in\mathbb{R}} \ f_{ij}(x_{ij}) + h(x_{ij}) \tag{21}$$

is the sub-problem that each prosumer needs to solve. Note that we can also approach (21) using the Gauss-Seidel or the Jacobi method. Since (21) is differentiable with respect to x_{ij}, finding a closed-form solution of x_{ij} would be more efficient.

The dual decomposition problem is now given by

$$\textbf{arg max}_{\{\lambda_i,\eta_j\}_{i,j\in\mathcal{N},\mathcal{N}_i}} \quad \mathcal{D}(\lambda,\eta) \qquad \forall i \in \mathcal{N}, \ \forall j \in \mathcal{N}_i. \tag{22}$$

A suitable method of solving (20) is the sub-gradient method [38]. Since the energy consumptions of different prosumers are decoupled, we adopt the sub-gradient technique to solve the problem in a distributed manner. The distributed solution further enhances the energy-saving opportunity of agentic AI and AI-ETA. Solving the sub-problem using the sub-gradient method gives the iterative solutions for λ_i and η_j as

$$\begin{aligned}\lambda_i^{k+1} &= \Big(\lambda_i^k + \hat{\tau}\nabla_{\lambda_i}\mathcal{D}\Big)^+ \\ &= \Big(\lambda_i^k + \hat{\tau}\Big(y_i - \sum_j x_{ij} - \sum_j \gamma_i x_{ij}^2\Big)\Big)^+\end{aligned} \tag{23a}$$

$$\eta_j^{k+1} = \Big(\eta_j^k + \hat{\tau}\nabla_{\eta_j}\mathcal{D}\Big)^+ = \Big(\eta_j^k + \hat{\tau}\big(\mathbb{C}_j - \sum_i x_{ij}\big)\Big)^+ \tag{23b}$$

where $\hat{\tau}$ is the step size. The values $x_{ij}^\star(\lambda_i,\eta_j)$ that minimise the Lagrangian in (20) are obtained as:

$$x_{ij}^\star(\lambda,\eta) = \textbf{arg min}_{x_{ij}\in\mathbb{R}} \ f_{ij}(x_{ij}) + h(x_{ij}). \tag{24}$$

The preceding problem is an unconstrained quadratic problem, and thus has a simple, closed-form solution. It can be easily shown that the solution is given by:

$$x_{ij}^\star(\lambda_i,\eta_j) = \frac{-\hat{b}_{ji} + \lambda_i + \eta_j}{2\hat{a}_{ji} - 2\gamma_i\lambda_i}. \tag{25}$$

The dual updates in (23a) and (23b) are implemented with projection onto $\mathbb{R}^+$ to ensure that $\lambda_i, \eta_j \geq 0$. For the simulations, $\hat{\tau}$ was chosen to be a small constant $\hat{\tau} = 0.05$ which was enough to yield stable convergence. Iterations are terminated when $||\lambda_{i+1} - \lambda_i||_2 \leq 10^{-4}$ and $||\eta_{j+1} - \eta_j||_2 \leq 10^{-4}$. The closed form solution $x_{ij}^\star(\lambda_i,\eta_j)$ in (25) is obtained from an unconstrained minimisation and can therefore take negative values. We therefore enforce the feasibility constraint $x_{ij} \geq 0$ by projecting $x_{ij}^\star(\lambda_i,\eta_j)$ into $max(0, x_{ij}^\star)$.

The optimal amount of energy sold in (25) depends on $\hat{b}_{ji}$, and is proportional to distance, ℓ_{ij}, informed by the SF of LoRaWAN based on agentic AI based on Algorithm 1.

B. Grid-Connected Prosumers

If some of the prosumers described above are also connected to the grid and unable to satisfy their non-flexible load E_i^{min}, requiring energy units $\sum_i x_{ij}$ to be procured from neighbours, they can buy the difference $(E_i^{min} - \sum_i x_{ij})$ from the grid. Let the grid energy price be ϱ_j, which varies with the location of the consumer from the grid. So, we can rewrite (4) as

$$\mathcal{T}_j^{(gm)}(x_{ij}) = \mathcal{T}_j(x_{ij}) + \sum_{j\in\mathcal{N}_i}\Big(E_i^{min} - \sum_{i\in\mathcal{N}} x_{ij}\Big)\varrho_j. \tag{26}$$

From (26), we can minimise the cost paid by the consumer as

$$\textbf{P2:} \quad \min_{\{x_{ij}\}} \sum_{j\in\mathcal{N}_i} \mathcal{T}_j^{(gm)}(x_{ij})$$

$$\text{subject to: (2), (18b)} \tag{27a}$$

$$\sum_{i\in\mathcal{N}} x_{ij} \geq 0, \ \forall j \in \mathcal{N}_i. \tag{27b}$$

Algorithm 1: Algorithm for optimising the virtual cluster size of P2P Energy by the agentic AI system with an insufficient number of energy prosumers per VMG

Input: $\{\mathcal{N} \mid \mathcal{N} = \mathcal{N}_c + \mathcal{N}_p\} > 0$
Output: $\{\text{SF} \mid d_i\} \leq 2r_m$

$\mathcal{N}_c \leftarrow define$;
$\mathcal{N}_p \leftarrow define$;
$\mathcal{N} \leftarrow \mathcal{N}_c + \mathcal{N}_p$;
$\text{SF} \leftarrow \{7, 8, \cdots, 12\}$; /* $|\text{SF}| = 6$, #SF used */
$n_k^{\text{SF}} \leftarrow define$; /* node threshold per SF */
$k \leftarrow \{1, \cdots, |\text{SF}|\}$; /* index of SF */
for $m \leftarrow 1$ **to** $\mathcal{M}$ **do**
  $\mathbf{V} \leftarrow \text{randi}([0\ \Phi], n, r)/r$; /* variable # prosumers */
  $n(m) \leftarrow \text{numel}(\mathbf{D}(\text{m}, :) \neq 0)$; /* #prosumers in m VMG */
  while $n \neq 0$ **do**
    while $n^m < n^{m+1}$ **do**
      if $n^{(m)} + n^{(m+1)} \leq n_6^{\text{SF}}$ **then**
        $\text{SF} \leftarrow 12$;
        $\text{VMG}_{(m+1)} \leftarrow \text{SF}$; /* Assign SF to VMG with higher node density */
        $\mathcal{T}_j(x_i^\star, d_i^\star) \leftarrow$ from (4) or (5)
      else
        if $n_6^{\text{SF}} < n^{(m)} + n^{(m+1)} \leq n_5^{\text{SF}}$ **then**
          $\text{SF} \leftarrow 11$;
          $\text{VMG}_{(m+1)} \leftarrow \text{SF}$;
          $\vdots$
        else
          if $\cdots < n_p^{(m)} + n_p^{(m+1)} \leq \cdots$ **then**
            $\vdots$
          else
            $\text{SF} \leftarrow 7$;
            $\text{VMG}_{(m+1)} \leftarrow \text{SF}$;
            $\vdots$
          end
        end
      end
    end
  end
end

Following the regime in Section III-A, we find that

$$\mathcal{D}^{(gm)}(\lambda_{ji}, \eta_{ji}) = \min_{x_{ij}} \mathcal{L}^{(gm)}(x_{ij}, \lambda_i, \eta_j) \tag{28a}$$

$$= \Psi^{(gm)}(x_{ij}) + \Phi^{(gm)}(x_{ij}). \tag{28b}$$

We note that $\Psi^{(gm)}(x_{ij}) \triangleq \Psi(x_{ij})$. However, $\Phi^{(gm)}(x_{ij}) \triangleq \Phi(x_{ij}) + \sum_{j\in\mathcal{N}_i} \left(E_i^{min} - \sum_{i\in\mathcal{N}} x_{ij}\right)\varrho_j$. From the first derivative of $\Phi^{(gm)}(x_{ij})$ and solving for η_j, we find that

$$x_{ij}^\star(\lambda_i, \eta_j) = \frac{-\hat{b}_{ji} + \lambda_i + \eta_j + \varrho_j}{2\hat{a}_{ji} - 2\gamma_i\lambda_i} \tag{29a}$$

$$\eta_j^{(gm)} = (2\hat{a}_{ji} - 2\gamma_i\lambda_i)x_{ij}^\star + \hat{b}_{ji} - \lambda_i - \varrho_j. \tag{29b}$$

From (29b), grid-connected prosumers will pay higher charges than off-grid prosumers as shown in Fig. 20.

C. Energy Cost Optimisation accounting for Communication Cost

To account for the additional communication cost component in (9), the energy cost objective is updated leading to

$$\textbf{P3:} \quad \min_{\{x_{ij}\}_{i,j\in\mathcal{N}}} \sum_{i\in\mathcal{N}} \sum_{j\in\mathcal{N}_i} \left(f_{ij}(x_{ij}) + C_{ji}^k(x_{ij})\right)$$

$$\text{subject to: (2), (18a), (18b).}$$

Based on this formulation, the corresponding Lagrangian function is constructed by introducing Lagrange multipliers. The Lagrangian of **P3** becomes

$$\begin{aligned}\mathcal{L}(x, \xi, \zeta) = &\sum_{i\in\mathcal{N}} \sum_{j\in\mathcal{N}_i} \left(f_{ij}(x_{ij}) + C_{ji}^k(x_{ij})\right) \\ &- \sum_{j\in\mathcal{N}} \xi_j \Big(\sum_{i\in\mathcal{N}_i} x_{ij} - \mathbb{C}_j \Big) \\ &+ \sum_{i\in\mathcal{N}} \zeta_i \Big(y_i - \sum_{j\in\mathcal{N}_i} x_{ij} - \sum_{j\in\mathcal{N}_i} \gamma_i x_{ij}^2 \Big)\end{aligned} \tag{31}$$

where $\boldsymbol{\zeta} \in \mathbf{R}_+^{|\mathcal{N}|}$ and $\boldsymbol{\xi} \in \mathbf{R}_+^{|\mathcal{N}_i|}$ are the Lagrangian multipliers. Minimising the Lagrangian leads to the following dual problem

$$\textbf{D3:} \quad \mathcal{D}(\lambda, \eta) = \inf_{\{x_{ij}\}_{i,j\in\mathcal{N}}} \mathcal{L}(x, \xi, \zeta) \tag{32a}$$

$$= \mathcal{G}(x_{ij}) + \mathcal{H} \tag{32b}$$

where

$$\mathcal{G}(x_{ij}) = \sum_{i\in\mathcal{N}} \sum_{j\in\mathcal{N}_i} g_{ij}, (\zeta_i, \xi_j),$$

$$\mathcal{H} = \sum_{i\in\mathcal{N}} \zeta_i y_i + \sum_{j\in\mathcal{N}_i} \xi_j \mathbb{C}_j,$$

and

$$g_{ij}(\zeta_i, \xi_j) = \arg\min_{x_{ij}\in\mathbb{R}} f_{ij}(x_{ij}) + C_{ji}^k(x_{ij}) + q(x_{ij}),$$

$$q(x_{ij}) = (-\zeta_i - \xi_j)x_{ij} - \zeta_i\gamma_i x_{ij}^2.$$

Given the separable structure of the dual problem, a sub-gradient method is employed to iteratively update the dual variables. Accordingly, the update equations for the Lagrange multipliers ζ_i and ξ_j are respectively given by

$$\begin{aligned}\zeta_i^{k+1} &= \left(\zeta_i^k + \tau\nabla_{\zeta_i}\mathcal{D}\right)^+ \\ &= \left(\zeta_i^k + \tau\left(y_i - \sum_j x_{ij} - \sum_j \gamma_i x_{ij}^2\right)\right)\end{aligned} \tag{33a}$$

$$\xi_j^{k+1} = \left(\xi_j^k + \tau\nabla_{\xi_j}\mathcal{D}\right)^+ = \left(\xi_j^k + \tau\left(\mathbb{C}_j - \sum_i x_{ij}\right)\right) \tag{33b}$$

where τ is the step size. The closed-form solution for problem (32b) is obtained by minimising the function

$$f_{ij}(x_{ij}) + C_{ji}^k(x_{ij}) + q(x_{ij}). \tag{34}$$

Assuming that $P_{t,k}(x_{ij})$ in (9) is differentiable, then minimising the function (34) is equivalent to solving for x_{ij} in

$$\hat{b}_{ji} - \zeta_i - \xi_j + (2\hat{a}_{ji} - 2\gamma_i\zeta_i)x_{ij} + \frac{\pi_e d_{ij}^k}{R} \cdot P_{k,t}^{'}(x_{ij}) = 0. \tag{35}$$

To gain further insight into the impact of communication costs, two representative forms of the communication cost function are considered.

1) Case 1: Linear Communication Cost: If the function $P_{t,k}(x_{ij})$ is linear, that is $P_{t,k}(x_{ij}) = p_0^k + p_1^k x_{ij}$, then the closed form solution (35) gives

$$x_{ij}^\star(\zeta_i, \xi_j) = \frac{-\hat{b}_{ji} + \zeta_i + \xi_j - \frac{\pi_e d_{ij}^k p_1^k}{R}}{2\hat{a}_{ji} - 2\gamma_i\zeta_i}.$$

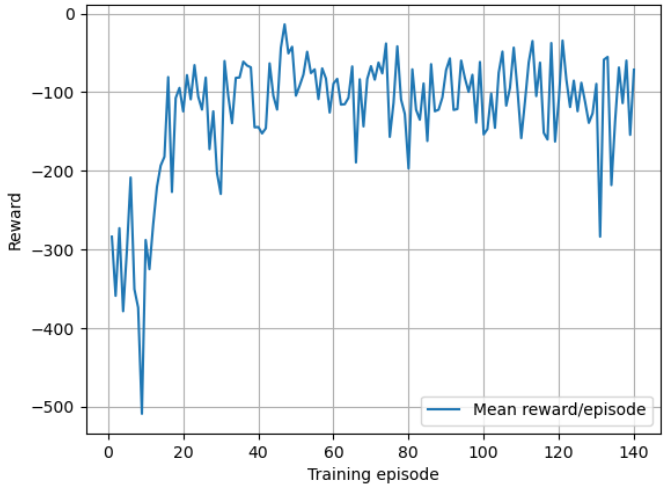

Figure 4: Reward received by AI agent during its training to guide it towards the learning goal.

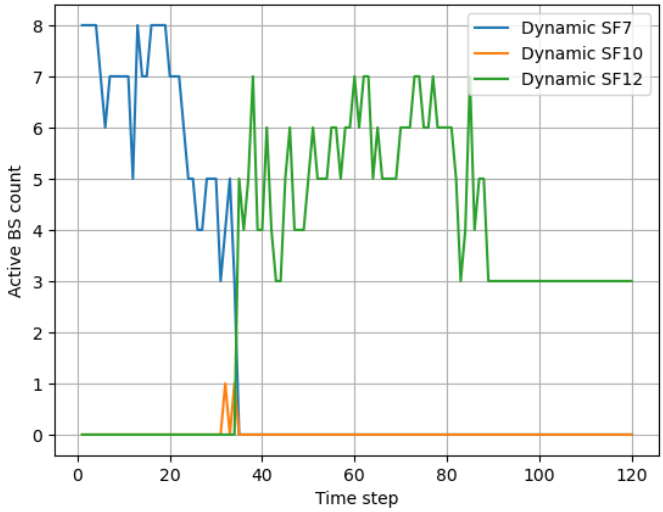

Figure 5: Active BTS count over trading time for different SF

If we let $\delta_{ij}^k = \frac{\pi_e d_{ij}^k}{R}$, we obtain the following

$$x_{ij}^{\star}(\zeta_i, \xi_j) = \frac{-\hat{b}_{ji} + \zeta_i + \xi_j - \delta_{ij}^k p_1^k}{2\hat{a}_{ji} - 2\gamma_i \zeta_i}. \tag{36}$$

2) Case 2: Quadratic Communication Cost: If the function $P_{t,k}(x_{ij})$ is quadratic, that is $P_{t,k}(x_{ij}) = p_0^k + p_1^k x_{ij} + p_2^k x_{ij}^2$, then the closed form solution (35) gives

$$x_{ij}^{\star}(\zeta_i, \xi_j) = \frac{-\hat{b}_{ji} + \zeta_i + \xi_j - \delta_{ij}^k p_1^k}{2\hat{a}_{ji} - 2\gamma_i \zeta_i + 2\delta_{ij}^k p_2^k}. \tag{37}$$

IV. Results and Discussion

As presented in Section II-B, we used Python software to create an instance of an AI agent based on reinforcement learning and the Q-learning algorithm (based on Bellman's model) to learn the traffic based on a 50 packets/day threshold. These AI agents predict the number of nodes available in a VMG. Each VMG uses its AI agent to report its node density to the central controller agentic AI system. The controller creates and updates its Q-table in the short memory as shown in Figure 3. The controller also maintains long-term memory that stores the SF status of local VMGs, i.e., the learned goals about the energy trading area. A planning tool is attached to the controller, from which the controller retrieves the reference SF and power-level parameters for each LoRaWAN station. Note that, assuming there is no need for global reconfiguration or zooming of VMGs, local AI agents can zoom individual VMGs using the proposed AI-ADR. Since local AI agents report to the controller agent, our presentation benefits from federated (or heuristic) reinforcement learning. We set a threshold for node density at which the controller switches the SF and transmit power, enabling AI-ADR. For example, at a count of n nodes per cluster, the controller switches to a lower (or higher) SF and power level, as appropriate. Note that LoRaWAN switches transmit power levels by 2dB when the SF is switched, according to TTN [51]. Packet loss was also monitored. During training, a reward is used to guide the agent toward the goal until it learned, as shown in Figure 4. Clearly, the agent learns to predict the number of prosumers in a VMG within 140 epochs using the received traffic data packets.

To demonstrate the numerical performance of the proposed models, we simulate scenarios with varying numbers of energy prosumers in a given trading area using MATLAB. By $area$, we denote a large P2P energy trading community in which prosumers are randomly distributed. To minimise costs, power losses and emissions in the area, we apply LoRaWAN coverage to group the energy traders into $1 \leq m \leq M$ VMGs. Each VMG is coordinated by an AI-ETA to optimise energy trading, reduce trading costs and increase value for money (utility). The VMGs equipped with LoRaWAN leverage the AI-ETAs with SF $\in \{7, 8, \cdots, 12\}$ to dynamically group prosumers into clusters. Since prosumers are typically fixed in location (except for EVs) and LoRaWAN coverage depends on the SF value, SF determines the number of prosumers that can coexist in one VMG. Other LoRaWAN parameters considered are defined in Section II-C. In Europe, $f = 868$MHz and larger bandwidth $W = 500$kHz is used as it is more interference-resilient and increases data rate [43]. We also assume that $\mu = 2$ and $c = 3 \times 10^8$m/s. The energy trading cost parameters $a = 1$, $b = 0.1$, $\alpha = 2 \times 10^{-2}$, $\beta = 0.1$, $\theta_{ji} = £0.25$ and $\varrho_{ji} = £0.3$ are used [14]. As described in (17), the traffic intensity received at the AI-ETA informs the number of energy prosumers present in a VMG at that time. Thus, following the examples in [34], the number of packets successfully transmitted to the AI-ETA by each prosumer is 50packets/day. Using a maximum transmit power of LoRaWAN, 14dB, the power varies with SF, falling in steps of 2dB following LoRaWAN Alliance datasheet [44, p.33]. The energy trading cost based on the dynamic model proposed is then evaluated. We also evaluate the effects of the distance between producers and consumers at each trading interval on the amount of energy sold within the given period. Next, we investigate the advantages of cell zooming on the energy trading cost performances.

A. Base Station Count, Power Consumption and OPEX

Using cluster zooming, Figure 5 demonstrates that there are more active base stations (LoRaWAN gateways) at lower SFs (e.g., SF7 and SF10) than at higher SFs (e.g., SF12). This phenomenon is expected: as the number of active prosumers increases, so does the number of active base stations required to support them. Compared with the non-dynamic design shown in Figure 6, the LoRaWAN BTSs consume 38.46% less power due to AI-assisted cell zooming during dynamic switching. In terms of OPEX, the dynamic AI-assisted cluster zooming reduces OPEX by 21.25%, as shown in Figure 7.

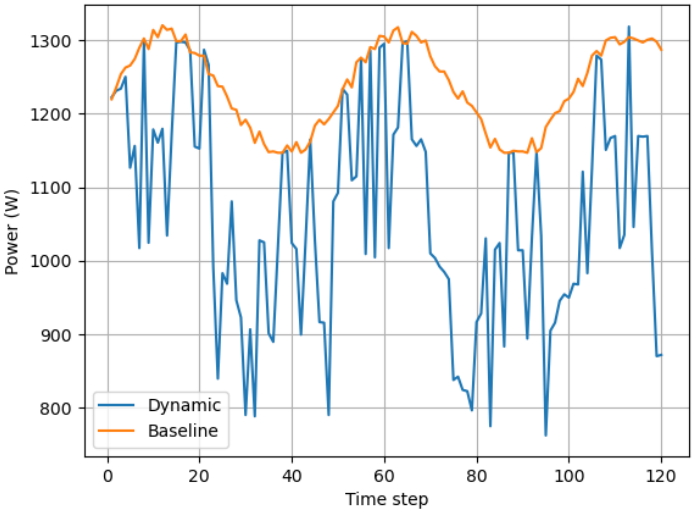

Figure 6: Power Consumption of static vs dynamic base stations

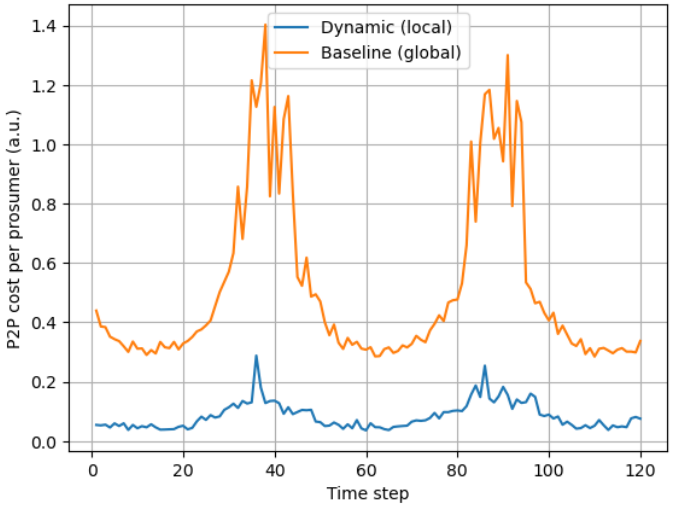

Figure 8: Overall P2P Energy Trading Cost Per Prosumer

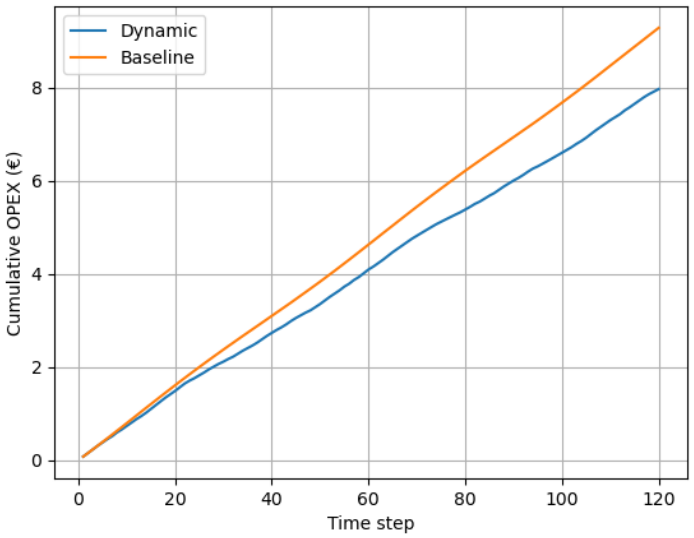

Figure 7: Cumulative operational expenditure for static and dynamic turning ON/OFF with agentic AI (AI-ADR) and conventional ADR

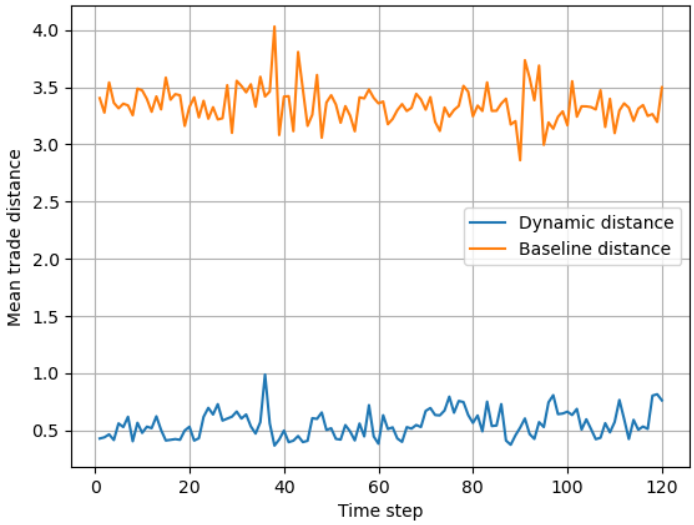

Figure 9: Effective energy trading distance covered during static vs dynamic clustering of energy prosumers.

B. P2P Energy Trading per Prosumer and Distance Reduced

The P2P energy trading cost for dynamic and non-dynamic scenarios is compared in Figure 8, showing about 50% reduction in P2P energy trading cost when the agentic AI cluster zooming was applied compared to when it was not. These results are due to the dynamic reduction in the average trading distance between seller and buyer in a VMG, which is shown in Figure 9. In Figure 10, the study demonstrates that the fees shared among the prosumers decrease with the number of prosumers. In other words, as the number of prosumers increases, the network switches from high SFs (e.g., SF12) to lower SFs (e.g., SF10 or SF7), and the energy trading cost due to prosumer sparsity scales with the number of prosumers, thereby reducing the cost. Similarly, in cell zooming, the proposed system zooms in to discover additional energy prosumers, thereby reducing fees shared among prosumers. For example, as the number of prosumers decreases, the network switches from low SFs (e.g., SF7) to higher SFs (e.g., SF10 or SF12), and the energy trading cost scales with new prosumers discovery, thereby reducing the cost. As shown in Figure 10, the fee-sharing scheme reduces the costs borne by individual prosumers as the number of prosumers discovered increases.

C. Coverage Count, AI-ADR, Packet Loss, Implied Coverage from Zooming

The number of active base stations based on coverage and count is shown in Figure 11. The resulting number of LoRaWAN base stations under the dynamic scenario is demonstrated in Figure 12. According to The Things Network (TTN) operated by The Things Industries, packet loss should exist within $0 - 10\%$ [51]. In this study, the packet error is presented in Figure 13. Clearly, the highest packet loss was observed in the dynamic clustering of VMGs with AI-ADR (9%), compared with the ideal case (0%). These results are consistent with the industry specification outlined by The Things Industries in [51] and outperform the 30% packet loss reported in [27] and 12% packet loss reported in [28].

D. Volumetric Analysis of Energy Traded

The goals of clustering, VMG zooming, and AI-assisted VMG zooming are to encourage local energy generation and participation, to convert passive energy consumers into active energy prosumers, to contribute to all-inclusive climate action, to reduce communication and energy trading OPEX for telecom operators,

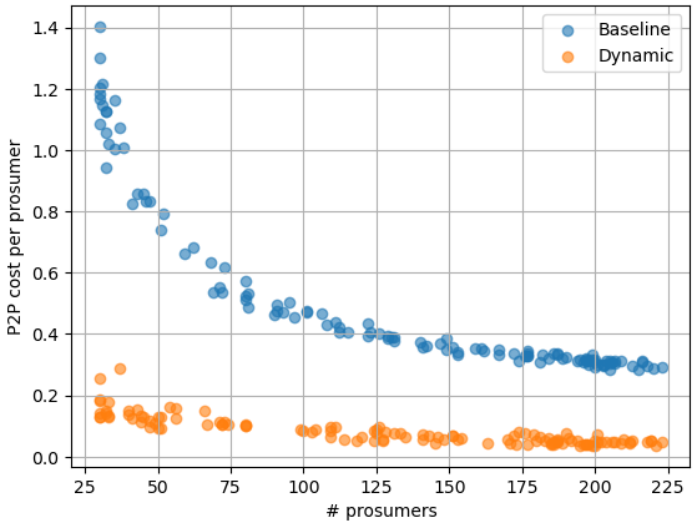

Figure 10: Fee sharing among discovered energy prosumers demonstrating that the cost paid by each prosumer reduces with the agentic AI-assisted cluster zooming than in static VMGs.

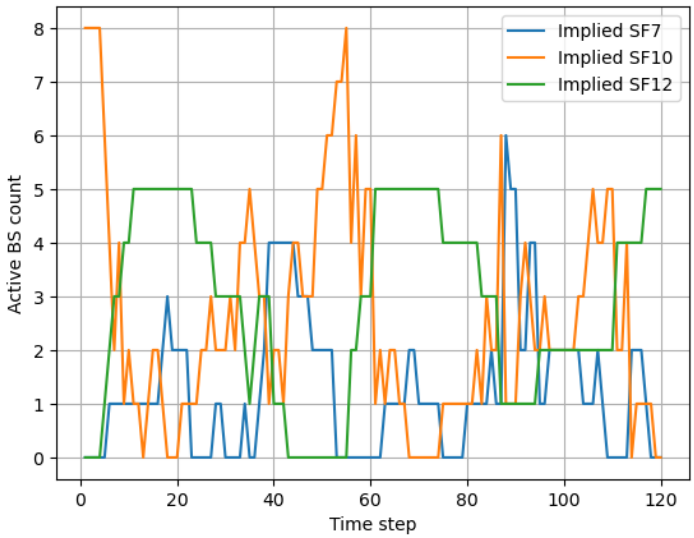

Figure 12: Implied SF from coverage zooming of the agentic AI-assisted cluster zooming.

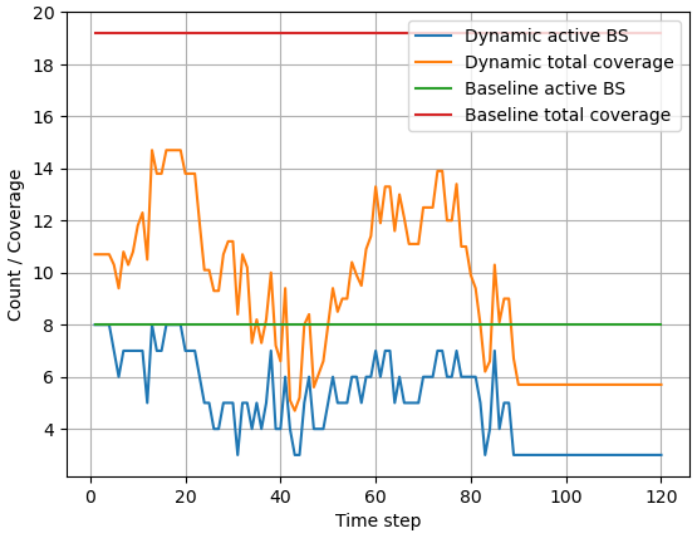

Figure 11: Wasted coverage Count of LoRaWAN reduces with the agentic AI-assisted cluster zooming than in static VMGs.

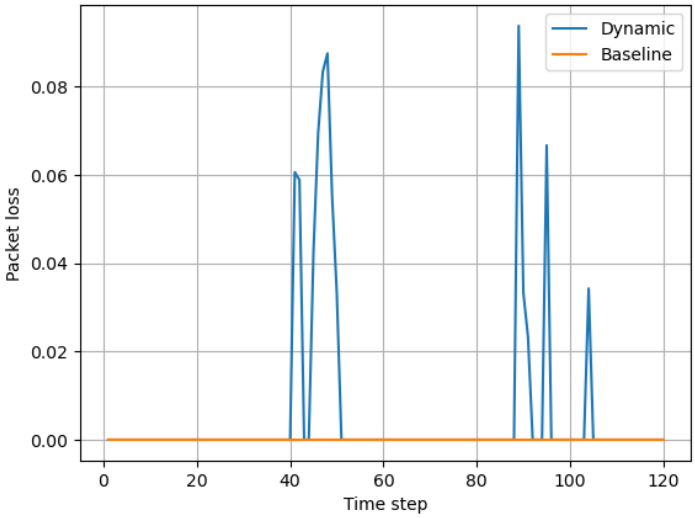

Figure 13: Packet loss with the agentic AI-assisted cluster zooming (with AI-ADR) compared with the ideal case.

and to minimise energy trading costs. Integrating AI agents, IoT and agentic AI into modelling and analysis of smart energy networks, and the forecasting of the example use case of future 6G network is not just innovative but transcedental with both economic and sustainability benefits. As shown in Figures 14 and 15, the volume of energy traded is more and closer to the prosumers than at further distances, with over 70% of the total energy sold in lower SFs.

E. Evaluation of Model Solution Convergence

A matrix of $x_{ij} \in \mathrm{X}$, shown in (3), represents the energy sold by prosumer i to prosumer j. It is a matrix of excess energy generated or stored by prosumer i. Using numerical simulation, the convergence of the trading parameters were investigated and shown in Figure 16, indicating the points where λ_i and η_j converge. Since the optimisation problem is convex with a strictly convex objective, convergence of the dual variables implies convergence to the unique primal optimal solution. To validate these optimal conditions, the L2 norms $\|\boldsymbol{\lambda}\|_2$ and $\|\boldsymbol{\eta}\|_2$ in Figure 16, respectively, show the point at which the solution of the energy price converges for each SF. In the simulation, the stopping criterion for the L2 norms, was set to 1×10^{-4}, that is $||\lambda_{i+1} - \lambda_i||_2 \approx 0$ and $||\eta_{j+1} - \eta_j||_2 \approx 0$.

F. Sensitivity Analysis: Energy Demand With Varying SF

In (23), a step size of $\hat{\tau} = 0.05$ is used, which suffices to achieve convergence. The simulations show optimised energy solutions, x^*_{ij}. Figure 17 shows prosumer j energy demand for a trading area with 5, 10, 50 and 100 prosumers, respectively, over different SF values. The results indicate that prosumer j demands higher energy amount at lower SF compared to higher SF. This shows that trading favours lower SF as this minimises trading distance and costs. AI-ETAs at each VMG use the high traffic volume to maintain the SF (i.e., energy trading cluster size). When the traffic volume changes, the agentic AI in the cloud uses local AI-ETA updates to reconfigure the cluster sizes. These results imply that a consumer is more motivated to procure energy from a nearby

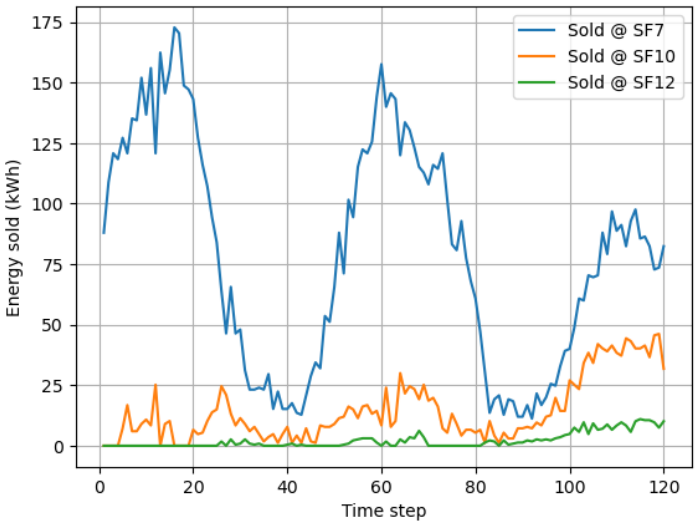

Figure 14: Energy sold in each SF when using the agentic AI-assisted cluster zooming (with AI-ADR).

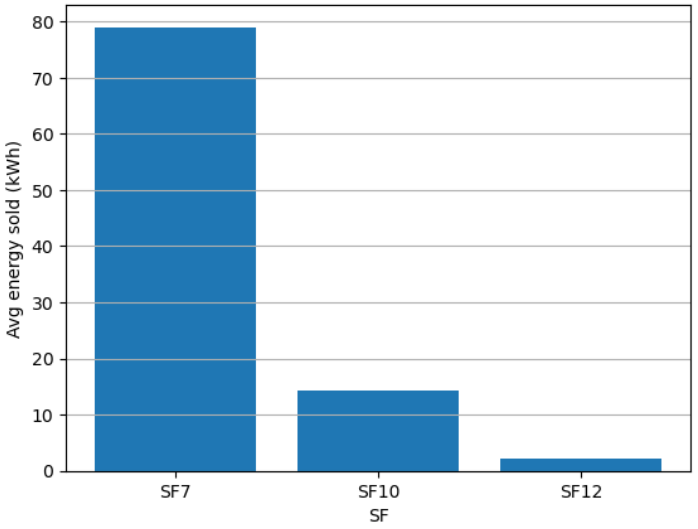

Figure 15: Average energy sold per SF when using the agentic AI-assisted cluster zooming (with AI-ADR) showing most energy sold in SF7.

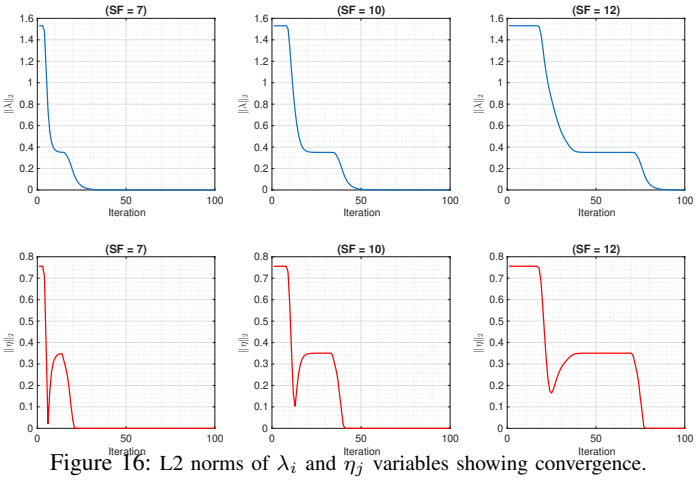

Figure 16: L2 norms of λ_i and η_j variables showing convergence.

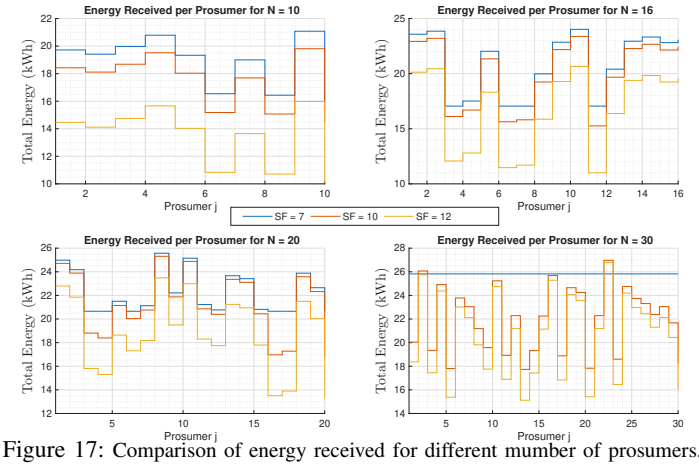

Figure 17: Comparison of energy received for different number of prosumers.

producer (e.g., within SF=7) rather than a farther one. Thus, the seller will realise higher revenue. In other words, higher volume of energy will be traded among producers and consumers in close proximity (e.g., within SF = 7 range), which results in higher revenue to the seller and lower cost to buyer. At longer distances (e.g., SF = 12), consumers are charged higher; consequently, less energy will be purchased, resulting in lower revenue for the producer, even with the same number of consumers. The results also show that the model enables a smart and environmentally sustainable energy trading community that encourages local area trading.

G. Average Energy Trading Cost Price Per Unit Energy

Traffic information received by the AI-ETA at each VMG is used to update the agentic AI in the cloud. Such data is used by the agentic AI to predict the optimal number of clusters and thus the cluster size, thereby minimising the average energy cost. In Figure 17, the results show that at farther distances from the prosumer (e.g. SF = 12), the quantity of energy sold is smaller (e.g. $x_{ij} = 13$ kWh) than at closer distances (e.g. SF = 7 with $x_{ij} = 18$ kWh), i.e., 38.46% with N = 10 prosumers and 40% with N=30 prosumers. This result from numerical simulation is comparable to that from the agentic AI implementation in Figures 14 and 15. The corresponding energy trading costs and average cost per unit energy are shown in Figures 18, indicating a higher average trading cost for higher SF. Correspondingly, consumers at extended distances from the producer pay a higher market price than closer ones, as shown in Figures 18. This is a well-known econometric principle, and in turn, prosumers could be motivated to trade locally rather than buy from distant prosumers. For 10 prosumers, trading in SF12 is 83.33% higher than in SF7. Similarly, trading in SF12 with 16, 20 and 30 prosumers is respectively 120%, 180% and 250% higher than in SF7. When normalised, the average cost decreases by up to 222.2% for SF12 as in Figure 19. However, as the number of prosumers increases, the cost reduces across all results in 18 and 19 (e.g., 40% for SF7, 25% for SF10 and 10.77% for SF12).

H. Impacts of Cell Zooming, Average Cost and Node Density

When the agentic AI system in the cloud determines the optimal cluster sizes, it passes instructions to AI-ETA on what SF to execute. We note that as the SF values increase, the coverage of the LoRaWAN increases; however, the amount of energy sold reduces due to larger distances and higher network charges - this encourages local energy trading. During cell zooming, the LoRaWAN can switch between different SF values depending on the number

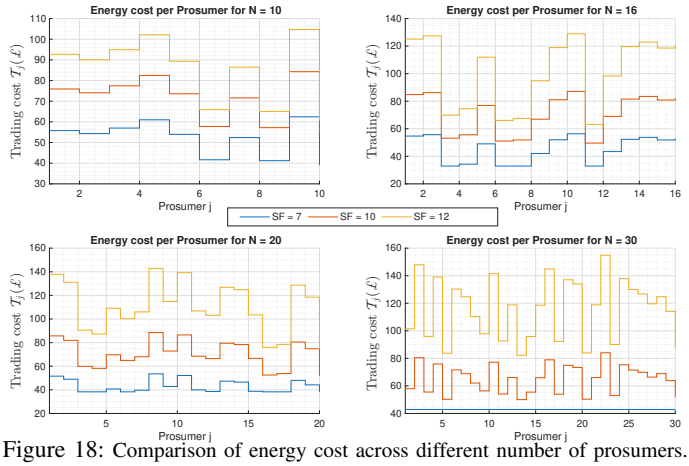

Figure 18: Comparison of energy cost across different number of prosumers.

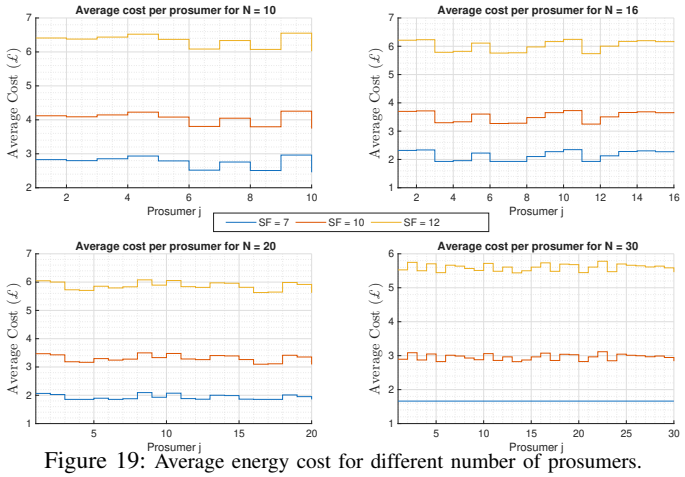

Figure 19: Average energy cost for different number of prosumers.

of prosumers available in the network at a given trading period. Usually, $\lambda_{\text{SF}} = 50$ packets/day [34] leads to $\Lambda_{\text{SF}} = 50n_t/A_{\text{SF}}$ node density. Based on (17), there is at least a 7.67% node density increase when SF switches due to cell zooming. If the trading becomes unfavourable that some prosumers defect, the LoRaWAN could switch from SF = 7 to 10 causing about 21.4% decrease in node density and from SF = 7 to 12 causing about 13.26% reduction in total sales as shown in Fig. 17. Switching the SF values is equivalent to increasing the coverage area, allowing some serving AI-ETAs and LoRaWAN stations to be switched off or put into sleep mode. Comparisons were also conducted for different numbers of prosumers, as shown in Figures 17, 18, and 19. These results indicate that the average costs generally decrease by 40% with an increase in the number of prosumers in a trading area.

I. Grid-Connected Prosumers

The energy price set by the grid is usually higher than the P2P energy price set by the participants in local energy communities [14]. As shown in Section IV, $\varrho_j > \theta_{ji}$. Since the energy prices between prosumers are private [4], [6], [38], AI-ETA uses traffic data to update the agentic AI system. In other words, AI-ETA and agentic AI systems do not include energy prices in deciding SF. From (26), the energy trading model includes the energy production charges from the grid $(E_j^{min} - \sum_j x_{ij})\varrho_j$ for prosumers to satisfy their minimum load. In this case, a typical producer behaves as a consumer. From Figure 20, it is seen that grid-connected prosumers (i.e., consumers in this case) pay higher energy charges than off-grid prosumers if they are unable to satisfy their minimum load requirement from the energy they produce.

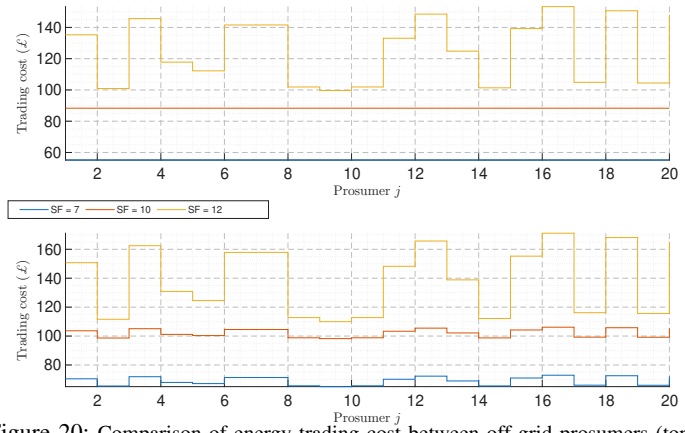

Figure 20: Comparison of energy trading cost between off-grid prosumers (top) and grid-connected prosumers (bottom) (across different SF for N=20) showing higher charges for grid-connected prosumers.

V. Conclusion

In this study, an agentic AI framework was applied to IoT to dynamically discover energy prosumers that can coexist in an energy trading cluster. Our goal was to develop a model that connects telecom distance and electrical distance (including power grid parameters, e.g., impedance, reactance and admittance), reduce trading distance autonomously, reduce trading cost, reduce power loss, optimise telecom resources, reduce operational expenditure, integrate emerging and pervasive technologies (e.g., IoT, machine learning, AI, cluster zooming) to automate energy networks, encourage P2P energy trading, local energy trading and embedded generation, and exemplify a possible use case that fits into the 3GPP requirement for the future 6G network involving the use of agentic AI system. In this study, we utilise network reconfigurability through an agentic AI cluster zooming to demonstrate how to reduce energy trading costs, network charges, and operating costs in energy trading when a smart microgrid is connected to the grid or not. The study shows that using an AI energy trading agent to dynamically adjust the logical energy trading area can enhance the discovery of energy subscribers and reduce energy trading charges. We demonstrated that leveraging SF values in LoRaWAN, combined with agentic AI cluster zooming, enables network reconfiguration in response to market variation. This approach facilitates the discovery of additional prosumers within the transactive network, resulting in a 40% reduction in trading costs. Hence, the proposed model is promising for optimising local area energy trading.

Acknowledgement

This paper was supported in part by the EPSRC grant Peer-to-Peer Energy Trading and Sharing - 3M (Multi-times, Multi-scales, Multi-qualities) with grant number EP/N03466X/1, and partly by the grant from EPSRC, REMARKABLE (EP/X039021/1) and the European Research Executive Agency (REA) Project 101086387.

References

[1] A. Alferidi, M. Alsolami, B. Lami, and S. B. Slama, "AI-Powered Microgrid Networks: Multi-Agent Deep Reinforcement Learning for Optimized Energy Trading in Interconnected Systems," *Arab. J. Sci. Eng.*, vol. 50, no. 8, pp. 6157–6179, 2025.

[2] M. N. Dehaghani, T. Korõtko, and A. Rosin, "AI applications for power quality issues in distribution systems: A systematic review," *IEEE Access*, 2025.

[3] O. Jogunola, A. Ikpehai, K. Anoh, B. Adebisi, M. Hammoudeh *et al.*, "State-of-the-art and prospects for peer-to-peer transaction-based energy system," *Energies*, vol. 10, no. 12, p. 2106, 2017.

[4] Z. Sun, Z. Li, Y. Li, X. Bai, J. Zhang, J. Zheng, and B. Deng, "Peer-to-peer energy trading with decentralized bidirectional matching of multipreference community prosumers," *Electr. Power Syst. Res.*, vol. 238, p. 111165, 2025.

[5] T. Morstyn, N. Farrell, S. J. Darby, and M. D. McCulloch, "Using peer-to-peer energy-trading platforms to incentivize prosumers to form federated power plants," *Nature Energy*, vol. 3, no. 2, p. 94, 2018.

[6] K. Erdayandi, L. C. Cordeiro, and M. A. Mustafa, "Privacy-preserving and accountable billing in peer-to-peer energy trading markets with homomorphic encryption and blockchain," *Sustain. Energy, Grids and Netw.*, vol. 41, p. 101568, 2025.

[7] K. Anoh, D. Bajovic, D. Vukobratovic, B. Adebisi, D. Jakovetic, and M. Cosovic, "Distributed energy trading with communication constraints," in *2018 IEEE PES ISGT-Europe*, Oct. 2018, pp. 1–6.

[8] S. A. Sadat and J. M. Pearce, "The threat of Economic Grid Defection in the US with Solar Photovoltaic, Battery and Generator Hybrid Systems," *Solar Energy*, vol. 282, p. 112910, 2024.

[9] L. Snyman, B. Bekker, M. L. Roux, and J. De Bruyn, "Financial, Regulatory, and Technical Perspectives on Residential Grid Defection in South Africa," in *33rd SAUPEC*, 2025, pp. 1–6.

[10] A. Navon, J. Belikov, R. Ofir, Y. Parag, A. Orda, and Y. Levron, "Death Spiral of the Legacy Grid: A Game-Theoretic Analysis of Modern Grid Defection Processes," *Iscience*, vol. 26, no. 4, 2023.

[11] Shawton Energy, "Your real energy cost: A guide to non commodity prices and passthrough costs," retrieved 05 Aug. 2025. [Online]. Available: https://shorturl.at/tY8kC

[12] D. Ashman, "Why non-commodity charges are driving your energy bill," Jun. 2025, retrieved 05 Aug. 2025. [Online]. Available: https://shorturl.at/lSRjk

[13] P. Allies, "Pass-through Contracts Explained," 2025, retrieved 05 Aug. 2025. [Online]. Available: https://www.powerfulallies.com/pass-through-contracts-explained/

[14] K. Anoh, S. Maharjan, A. Ikpehai *et al.*, "Energy Peer-to-Peer Trading in Virtual Microgrids in Smart Grids: A Game-Theoretic Approach," *IEEE Trans. Smart Grid*, vol. 11, no. 2, pp. 1264–1275, 2020.

[15] K. Anoh, A. Ikpehai, D. Bajovic, O. Jogunola, B. Adebisi, D. Vukobratovic, and M. Hamoudeh, "Virtual microgrids: A management concept for peer-to-peer energy trading," in *ICFNDS*, 2018.

[16] A. Paudel, L. P. M. I. Sampath, J. Yang, and H. B. Gooi, "Peer-to-Peer Energy Trading in Smart Grid Considering Power Losses and Network Fees," *IEEE Trans. Smart Grid*, pp. 1–1, 2020.

[17] D. B. Acharya, K. Kuppan *et al.*, "Agentic AI: Autonomous intelligence for complex goals–a comprehensive survey," *IEEE Access*, 2025.

[18] A. K. Pati, "Agentic AI: A Comprehensive Survey of Technologies, Applications, and Societal Implications," *IEEE Access*, 2025.

[19] Y. Abadade, A. Temouden, H. Bamoumen, N. Benamar, Y. Chtouki, and A. S. Hafid, "A comprehensive survey on TinyML," *IEEE Access*, vol. 11, pp. 96 892–96 922, 2023.

[20] A. Ikpehai, B. Adebisi, K. M. Rabie, K. Anoh, R. E. Ande, M. Hammoudeh, H. Gacanin, and U. M. Mbanaso, "Low-Power Wide Area Network Technologies for Internet-of-Things: A Comparative Review," *IEEE IoT J.*, vol. 6, no. 2, pp. 2225–2240, Apr. 2019.

[21] D. C. Nguyen, M. Ding, P. N. Pathirana, A. Seneviratne, J. Li, D. Niyato, O. Dobre, and H. V. Poor, "6G Internet of Things: A comprehensive survey," *IEEE IoT J.*, vol. 9, no. 1, pp. 359–383, 2021.

[22] R. Singh, A. Kaushik, W. Shin, M. Di Renzo, V. Sciancalepore, D. Lee, H. Sasaki *et al.*, "Towards 6G evolution: Three enhancements, three innovations, and three major challenges," *IEEE Netw.*, 2025.

[23] K. Anoh, D. Bajovic, A. Ikpehai, B. Adebisi, and D. Vukobratovic, "Enabling Peer to Peer Energy Trading in Virtual Microgrids with LP-WAN," in *18th IEEE EUROCON, Serbia, Jul. 1-4*, 2019.

[24] Z. Niu, Y. Wu, J. Gong, and Z. Yang, "Cell zooming for cost-efficient green cellular networks," *IEEE Commun. Mag.*, vol. 48, no. 11, pp. 74–79, Nov. 2010.

[25] N. Chinchilla-Romero, J. Navarro-Ortiz, F. Delgado-Ferro, and J. M. Lopez-Soler, "6G-LoRaGRAN: A Testbed for Researching LoRaWAN and 5G Integration," in *IEEE WCNC*, 2025, pp. 1–7.

[26] K. Anoh, B. Kipchumba, O. Okpako, A. Ikpehai, K. C. Okafor, and S. Maharjan, "Use Case of Agentic AI and IoT in 6G Networks for P2P Energy Trading in Smart Grids," in *1st Int. Conf. Artif. Intell. Sustain. Cities (AI-Scities), Bognor Regis, UK*, 2025.

[27] A. Prakash, N. Choudhury, A. Hazarika, and A. Gorrela, "Effective Feature Selection for Predicting Spreading Factor with ML in Large LoRaWAN-based Mobile IoT Networks," in *Nation. Conf. Communic.*, 2025, pp. 1–6.

[28] L. Leonardi, G. Iannizzotto, M. Pirri, G. Patti, A. Pirri, and L. L. Bello, "A Deep Learning-Based Adaptive Data Rate Algorithm for LoRaWAN Networks," *IoT*, p. 101786, 2025.

[29] O. Jogunola, B. Adebisi, K. Anoh, A. Ikpehai, M. Hammoudeh, and G. Harris, "Multi-commodity optimization of peer-to-peer energy trading resources in smart grid," *J. Modern Power Systems and Clean Energy*, vol. 10, no. 1, pp. 29–39, 2021.

[30] A. Izanlo, S. A. Gholamian, A. Sheikholeslami, M. Khorasany, M. V. Kazemi, and A. Iqbal, "Analytical Examination of Strategic and Purposeful Behaviours in Peer-to-Peer Energy Trading," *IET Gen., Trans. & Distr.*, vol. 20, no. 1, 2026.

[31] O. Jogunola, B. Adebisi, K. Anoh, A. Ikpehai, M. Hammoudeh *et al.*, "Distributed Adaptive Primal Algorithm for P2P-ETS over Unreliable Communication Links," *Energies*, vol. 11, no. 9, p. 2331, 2018.

[32] S. Maharjan, Y. Zhang, S. Gjessing, and D. Tsang, "User-centric demand response management in the smart grid with multiple providers," *IEEE Trans. Emerging Topics Comput.*, vol. 5, no. 4, pp. 494–505, Oct. 2017.

[33] J. Petajajarvi, K. Mikhaylov, A. Roivainen, T. Hanninen *et al.*, "On the coverage of LPWANs: range Evaluation and Channel Attenuation Model for LoRa Technology," in *2015 14th ITST*, 2015, pp. 55–59.

[34] D. Vukobratovic, D. Bajovic, K. Anoh, and B. Adebisi, "Distributed Energy Trading via Cellular Internet of Things and Mobile Edge Computing," in *ICC 2019 - IEEE Intl. Conf. Commun.*, May 2019.

[35] E. Calvano, G. Calzolari, V. Denicolo, and S. Pastorello, "Artificial Intelligence, Algorithmic Pricing, and Collusion," *American Economic Review*, vol. 110, no. 10, pp. 3267–3297, 2020.

[36] O. Jogunola, M. Hammoudeh, B. Adebisi, and K. Anoh, "Demonstrating blockchain-enabled peer-to-peer energy trading and sharing," in *IEEE Canadian Conf. Electric. Comput. Engineer.*, 2019, pp. 1–4.

[37] P. A. Olujimi, P. A. Owolawi, R. C. Mogase, and E. V. Wyk, "Agentic AI frameworks in SMMEs: A systematic literature review of ecosystemic interconnected agents," *AI*, vol. 6, no. 6, p. 123, 2025.

[38] P. Samadi, A. Mohsenian-Rad, R. Schober, V. Wong, and J. Jatskevich, "Optimal real-time pricing algorithm based on utility maximization for smart grid," in *First IEEE smartgridcomm*, Oct. 2010, pp. 415–420.

[39] K. Anoh, C. H. See, Y. Dama, R. A. Abd-Alhameed, and S. Keates, "6G wireless communication systems: applications, opportunities and challenges," *Future Internet*, vol. 14, no. 12, p. 379, 2022.

[40] M. K. Shehzad, L. Rose, M. M. Butt, I. Z. Kovacs, M. Assaad, and M. Guizani, "Artificial intelligence for 6G networks: Technology advancement and standardization," *IEEE Vehic. Technol. Magaz.*, vol. 17, no. 3, pp. 16–25, 2022.

[41] Y. Gao, A. Centonza, and G. Cao, "AI/ML for NG-RAN & 5G-Advanced towards 6G," Aug. 2025, retrieved 06 Sept. 2025. [Online]. Available: https://www.3gpp.org/technologies/ai-ml-ngran

[42] T. Bouguera, J. Diouris, J. Chaillout, R. Jaouadi, and G. Andrieux, "Energy consumption model for sensor nodes based on LoRa and LoRaWAN," *Sensors*, vol. 18, no. 7, p. 2104, 2018.

[43] T. Voigt, M. Bor, U. Roedig, and J. Alonso, "Mitigating inter-network interference in LoRa networks," *arXiv preprint arXiv:1611.00688*, 2016.

[44] LoRa Alliance Technical Committee, *LoRaWAN Regional Parameters RP002-1.0.4*, LoRa Alliance, Fremont, CA, USA, Sep. 2022, ver. 1.0.4. [Online]. Available: https://resources.lora-alliance.org/technical-specifications/rp002-1-0-4-regional-parameters

[45] F. T. Ulaby and U. Ravaioli, *Fundamentals of Applied Electromagnetics*. Pearson Upper Saddle River, NJ, 2022, vol. 8.

[46] J. D. Glover, M. S. Sarma, T. J. Overbye, and B. Adam, *Power system analysis and design*, 7th ed. Cengage Learning Stamford, CT, USA, 2022.

[47] D. Moltchanov, "Distance Distributions in Random Networks," *Ad Hoc Netw.*, vol. 10, no. 6, pp. 1146–1166, 2012.

[48] M. Haenggi, "On Distances in Uniformly Random Networks," *IEEE Trans. Inf. Theory*, vol. 51, no. 10, pp. 3584–3586, Oct. 2005.

[49] G. Last and M. Penrose, *Lectures on the Poisson process*. Cambridge University Press, 2018, vol. 7.

[50] M. J. Kochenderfer and T. A. Wheeler, *Algorithms for Optimization*. MIT Press, 2025.

[51] The Things Industries, *Hardware*, 2026. [Online]. Available: https://www.thethingsindustries.com/docs/hardware/devices/concepts/best-practices/